Structured illumination photoacoustic imaging using Hadamard encoding

Paltauf G(1)*, Torke PR(1), Mack F(1), Nuster R(1)

(1) Department of Physics, University of Graz, Graz, Austria

*Corresponding author's email: guenther.paltauf@uni-graz.at

Photoacoustic microscopy with optical resolution (OR-PAM) is a method to visualize structures with optical absorption contrast in biological samples [1]. To acquire images, short laser pulses are focused with an objective into the target and are scanned over the imaging plane. The generated acoustic signals are received by an ultrasound sensor. The optical focusing gives a lateral resolution comparable to purely optical microscopy. Due to the small focal area, high fluence values are achieved within the absorbing structures (e.g. blood capillaries), ranging up to 1 J/cm², even if the pulse energy is in the nanojoule range and the radiant exposure on the sample surface is below the ANSI limit for biological tissue. In some biomedical applications, such high fluence values are not desirable or cannot be generated, either due to the potential damage to delicate tissue structures or due to the poor focusing capabilities of the light source.

To enable OR-PAM with much lower fluence values, we propose a technique based on structured illumination of the sample and integrated detection of the resulting acoustic wave. Using methods from computational ghost imaging (GI), the parallel detection of acoustic signals generated over an extended area should give higher signals and better signal-to-noise ratio (SNR) than conventional pixelwise scanning, even if the applied fluence is lower [2]. This is the result of the multiplex advantage, which has been exploited in various imaging scenarios [3,4].

Structured illumination is achieved by projecting patterns obtained from a Hadamard matrix via a digital micromirror device (DMD) onto the object. For an n x n-pixel image, the patterns are obtained from a Hadamard matrix **H** of size n^2 x n^2. After replacing elements equal to -1 by zeros, lines of the matrix are reformatted to the required n x n size for projection. With a depth-dependent fluence (z), the energy density W and initial pressure p_0 generated by heating an object with an absorption coefficient distribution μ_a are given by

$$p_0(x,y,z) = \Gamma W(x,y,z) = \Gamma \Psi(z)\, h_i(x,y)\, \mu_a(x,y,z) \qquad \text{Eqn. 1}$$

where $h_i(x,y)$ is the pattern generated by the i-th row of **H** and is the Grüneisen parameter. Assuming that the recorded pressure signal $s(t)$ is proportional to the initial pressure $p_0(x,y,z = c_s t)$, where c_s is the speed of sound, an image representing the energy density distribution at given depth is reconstructed by

$$I(x,y,z) = \sum_n h_n(x,y)\, s_n\left(t = z/c_s\right) \qquad \text{Eqn. 2}$$

For better performance, the differential ghost imaging method was applied [5], where s_n is the difference between two signals recorded after projecting the original pattern and its inverse, where zeros and ones are swapped. Equation (2) corresponds to a multiplication of the original matrix **H** with a signal representing a multiplication of **H** by the μ_a - distribution weighted with the depth-dependent fluence. Owing to the self-inverse property of **H**, this gives a close representation of the μ_a-distribution.

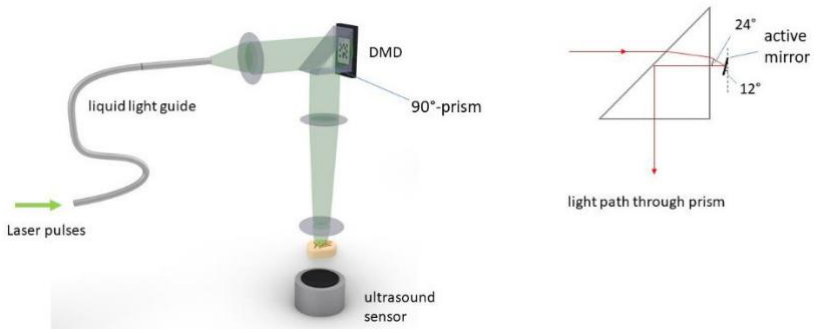

Fig. 1. Experimental setup for ghost imaging. The detail shows how light is reflected by an active mirror on the DMD and redirected via the prism to the sample. An ultrasound sensor with a center frequency of 3.5 MHz records the generated pressure signals.

To test the imaging method, pulses from a 515-nm, nanosecond-pulsed laser were projected via a DMD and an objective lens onto a phantom consisting of black carbon fibers embedded in transparent gel-wax. The setup is shown schematically in Fig.1. Projected patterns had a size of 64 x 64 pixel. A reconstruction for a selected depth is shown in Fig.2a. To demonstrate the performance of the GI approach in comparison with conventional pixelwise scanning, the same phantom was imaged again, activating only a single pixel on the DMD at a time. The result is shown in Fig.2b. In both experiments, the fluence arriving at the absorbing target was about 1.3 mJ/cm². Figure 3c shows the maximum amplitude projection (MAP) image together with a photograph of the phantom.

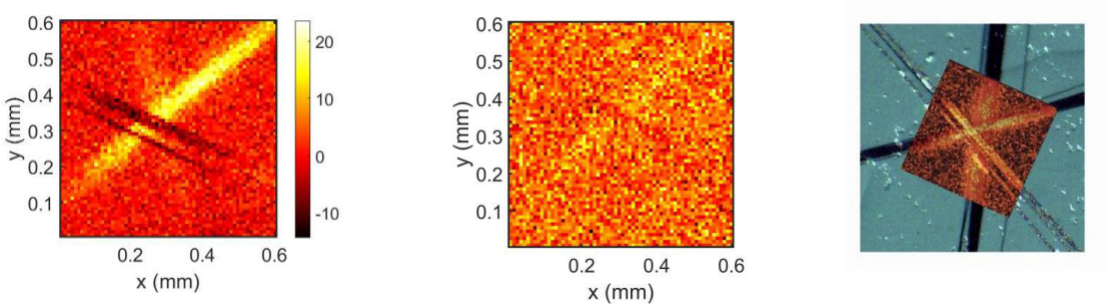

Fig. 2. images of a carbon fiber phantom with (a) the GI technique, (b) using single-pixel scanning. (c) Shows the phantom, together with a maximum amplitude projection of the GI reconstruction.

These results demonstrate that despite the extremely low incident fluence the GI method still gives satisfactory imaging contrast in comparison to the pixelwise raster scan, where hardly any structures can be perceived. Since the fiber bundles are separated in depth by less than the axial resolution of the ultrasound sensor, the image in Fig. 2a is overlain by an artifact generated by a bundle located a different depth.

The expected depth range of the GI technique in real tissue was investigated in a simulation, where a Monte Carlo method was used to calculate the initial pressure distribution in a phantom containing “blood vessels” at different depths. A detail of the energy density distribution in the phantom is displayed in Fig.3a with logarithmic scaling. In this section, the structured illumination can be observed to a depth of about 400 µm. Nevertheless, as the MAP in Fig.3b demonstrates, even structures at a depth of 760 µm can be recognized in the reconstruction, albeit with very low contrast.

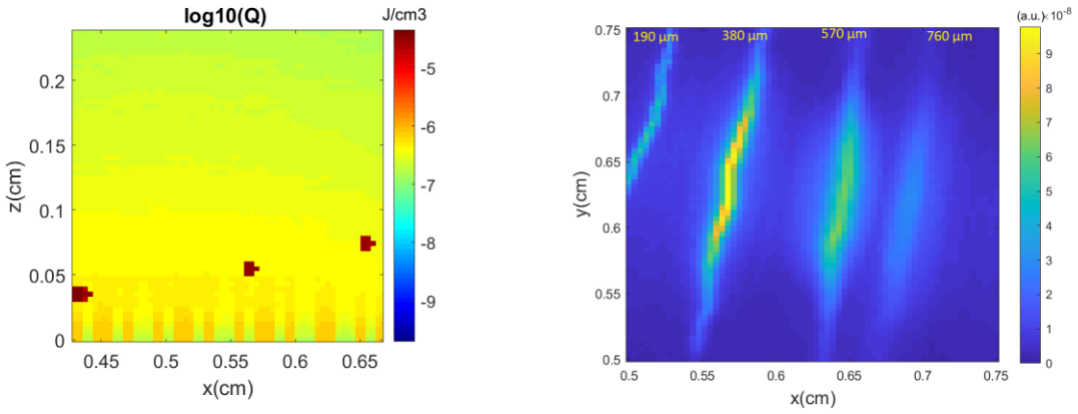

Fig. 3. Simulation results, showing GI of a vessel-phantom. (a) Cross sectional image of the energy density distribution, showing a close-up of the phantom with three "blood vessels" at different depths. (b) Maximum amplitude projection of the reconstructed image, showing some contrast even for the deep vessel located at 760 µm depth.

In conclusion, structured illumination combined with GI reconstruction is able to generate images with much better contrast compared to a raster scan image at the same radiant exposure. This could be of practical use in applications where the exposure is limited, either because of safety precautions or of the properties of the light source. In particular, photoacoustic GI will enable the use of light sources, which cannot be focused to the small spot size required in conventional OR-PAM.

Acknowledgments – This work has been supported by the Austrian Research Promotion Agency (FFG), Project No. 874787.

References

[1] S. Jeon, J. Kim, D. Lee, J. W. Baik, and C. Kim, Review on practical photoacoustic microscopy, Photoacoustics 15 (2019) 10014. https://doi.org/10.1016/j.pacs.2019.100141.

[2] O. Katz, Y. Bromberg, Y. Silberberg, Compressive ghost imaging, Appl. Phys. Lett. 95 (2009) 131110. https://doi.org/10.1063/1.3238296.

[3] J. Liang, L. Gao, C. Li, and L. V. Wang, Spatially Fourier-encoded photoacoustic microscopy using a digital micromirror device, Optics letters 39 (2014) 430–433. https://doi.org/10.1364/OL.39.000430.

[4] T.J. Lane, D. Ratner, What are the advantages of ghost imaging? Multiplexing for x-ray and electron imaging, Opt.Express 28 (2020) 5898–5918. https://doi.org/10.1364/OE.379503.

[5] B. Sun, M.P. Edgar, R. Bowman, L.E. Vittert, S. Welsh, A. Bowman, MJ. Padgett, Differential Computational Ghost Imaging, in Imaging and Applied Optics, OSA Technical Digest (online), CTu1C.4.